Engineered periosteum-diaphysis substitutes with biomimetic structure and composition promote the repair of large segmental bone defects

Lili Yu[a,1], Qiang Wei[a,1], Jiaying Li[a], Huan Wang[a], Qingchen Meng[a], En Xie[a], Zexi Li[a], Kexin Li[a], Wenmiao Will Shu[b], Junxi Wu[b], Lei Yang[a,c], Yan Cai[a,***], Fengxuan Han[a,**], Bin Li[a,*]

[a] College of Chemistry, Chemical Engineering and Materials Science, Orthopedic Institute, Department of Orthopaedic Surgery, The First Affiliated Hospital, Suzhou Medical College, Soochow University, Suzhou, Jiangsu, China

[b] Department of Biomedical Engineering, University of Strathclyde, Glasgow, G1 1QE, UK

[c] Center for Health Sciences and Engineering (CHSE), School of Health Sciences and Biomedical Engineering, Hebei University of Technology, Tianjin, China

[1] Lili Yu and Qiang Wei contributed equally to this work and shared the first authorship.

[*] Corresponding author.

[**] Corresponding author.

[***] Corresponding author.

[*] Corresponding to:

Prof. Bin Li, Rm 201 Bldg Jiwu, Soochow University (North Campus), 178 Ganjiang Rd, Suzhou, Jiangsu 215007, China

Tel. & Fax: (+86) 512-6778-1163

E-mail addresses: binli@suda.edu.cn (Bin Li), fxhan@suda.edu.cn (Fengxuan Han), wcy65168299@163.com (Yan Cai).

This is a peer-reviewed, accepted author manuscript of the following paper: Yu, L., Wei, Q., Li, J., Wang, H., Meng, Q., Xie, E., Li, Z., Li, K., Shu, W. W., Wu, J., Yang, L., Cai, Y., Han, F., & Li, B. (2023). Engineered periosteum-diaphysis substitutes with biomimetic structure and composition promote the repair of large segmental bone defects. Composites Part B: Engineering, 252, [110505]. https://doi.org/10.1016/j.compositesb.2023.110505

Abstract

The repair of large segmental bone defects remains a big challenge due to limited self-healing capacity of bone. Digging into the structure and composition of natural long bone let us realize that the periosteum cambium on the surface of diaphysis plays a crucial role in bone repair. In this study, we explored the feasibility of using a tissue-engineered periosteum-diaphysis substitute to repair the large segmental bone defects. To create an artificial periosteum cambium, bone marrow mesenchymal stem cells (BMSCs) and endothelial progenitor cells (EPCs) were co-cultured on electrospun silk fibroin (SF) fibrous membranes for mimicking the cellular composition and microstructure of cambium layer of the native periosteum. These SF membranes supported the adhesion and proliferation of both BMSCs and EPCs. In addition, we found that a 1:1 ratio of BMSCs and EPCs supported osteogenesis and angiogenesis optimally. This biomimetic periosteum layer was integrated with artificial diaphysis made of tubular SF scaffolds to construct a biomimetic periosteum-diaphysis substitute. Animal studies confirmed that the biomimetic periosteum-diaphysis substitutes promoted the repair of critical-size bone defects of rabbit radius. Furthermore, the transplanted biomimetic periosteum-diaphysis substitute could prevent the growth of fibrous tissues in the bone defect, and thus reduce the occurrence of nonunion. This study described a promising tissue engineering strategy for the repair of large segmental bone defects.

Keywords: Silk fibroin; Electrospun membrane; Periosteum cambium; Diaphysis; Bone repair

1. Introduction

More than two million Americans suffer from large bone defects annually, and ~5% of them require medical intervention to heal [1]. Currently, the treatment of large bone defects remains a tough challenge, largely due to hypoxia and nutrient deficiency [2]. The diaphysis, main portion of the bone, will face more severe nutritional deficiencies than other parts of long bone after large segmental bone injury, which make its repair a big challenge. It is reported that 5-10% of patients with large segmental bone defects will be disabled due to the delayed union or nonunion of the broken fragments [3]. Current treatments involve autologous and allogeneic bone transplantation. However, the shortage of donor, ethical concerns, and the worrying survival of transplants limit the effectiveness of these treatments [4, 5]. In the past decade, many attempts have been made in bone tissue engineering to promote the repair of bone defects with scaffolds in combination with osteoprogenitor cells. However, these engineered scaffolds show suboptimal curative effect due to the lack of progenitor cells and vascular network, which often leads to tissue necrosis [6].

The long bone consists mainly of the diaphysis and periosteum covering the surface. In the traditional management of large bone defects, the focus was on the repair of diaphysis, while the importance of periosteum was often overlooked. However, recent studies demonstrated that the removal of bone marrow progenitor cells had a negligible effect on bone regeneration, while the loss of periosteum led to a 73% reduction in new bone formation [7]. The periosteum is a fibrous connective tissue membrane which has

two unique layers. The outer fibrous layer is mainly composed of fibroblasts and collagen fibers which provide support and protection for the periosteum and bone. The inner layer, also known as cambium layer, contains H-type vascular endothelial cells and various progenitor cells that are directly associated with osteogenesis. The cambium layer also provides essential nutrients for bone regeneration [8]. Thus, the remodeling of periosteum is increasingly being considered as a critical component in the treatment of severe fractures and the prevention of nonunion.

Given this change in direction, tissue-engineered periosteum is increasingly being used to repair large segmental bone defects [9]. Current tissue-engineered periosteum scaffolds are made of acellular dermis, cell sheets, hydrogels, electrospun membranes, and porcine small intestinal submucosa. However, these structures fail to replicate the role of promoting osteogenesis and angiogenesis compared to the natural periosteum. For example, some bioactive factors were directly added to these materials [10]. However, these attempts often led to adverse outcomes such as inflammation and immune responses [11, 12], excessive, or ectopic osteogenesis [13]. Another strategy is to use the artificial periosteum as a vehicle to deliver drugs to enhance its osteogenic potential [14, 15]. This strategy has improved the solubility and bioavailability of poorly soluble drugs to a certain extent, but there are still limitations such as clearance by the body, insufficient targeting efficiency, poor carrier safety and tissue permeability. Therefore, it is an urgent need to develop an artificial periosteum that mimics the natural cambium layer providing cellular components and necessary growth factors for osteogenesis and angiogenesis.

The unsatisfactory results of periosteum tissue engineering partly attribute to the lack of cellular components. Bone marrow mesenchymal stem cells (BMSCs) are the most widely used cells in bone tissue engineering, which have the potential to differentiate into osteoblasts [16, 17]. Endothelial progenitor cells (EPCs) have been shown to promote bone healing due to their excellent pro-angiogenic capacity. Studies have shown that the co-culture of BMSCs and EPCs can synergistically promote osteogenesis and angiogenesis [18], however, the optimal ratio between the two types of cells remains disputed and needs to be further confirmed experimentally.

Silk fibroin (SF) is a natural fibrin extracted from the cocoons of silkworm and has excellent biocompatibility, biodegradability, and good mechanical properties [19]. It demonstrates tunable mechanical properties comparable to various tissues, making it a suitable material in bone tissue engineering. Electrospinning is a simple and widely available technology that can be used to prepare fibrous membrane with a microstructure similar to the natural periosteum [20, 21]. In addition, large segmental bone repair also requires a scaffold to maintain the structural stability. The diaphysis of long bone is hollow inside, with a porous tubular structure. Directional freeze drying is a technology for the fabrication of scaffolds with directional pores that could mimic the microstructure of diaphysis [22]. This technology enables the creation of tubular SF structures with directional pores by means of suitable molds. As reported previously, scaffolds with directional pores are more conducive to the infiltration and migration of surrounding cells, the exchange of nutrients and metabolic wastes, and the deposition of extracellular matrix

[23, 24]. Inspired by the structure of natural long bone, the design of biomimetic bone substitutes for the promotion of bone repair is now becoming possible.

In this study, we developed tissue-engineered periosteum-diaphysis grafts for the repair of large segmental bone defects. The scaffold is composed of cell-laden SF electrospun fibrous membranes which mimic the microstructure and cellular composition of the cambium layer of periosteum. In addition, tubular SF scaffolds with hollow channels and aligned micropores were prepared by directional freeze-drying to mimic the natural structure of diaphysis. Firstly, different proportions of BMSCs and EPCs were co-cultured on electrospun SF membranes and then the optimal ratio of BMSCs and EPCs was screened for the following experiments. Subsequently, the membranes seeded with cells (MC) were wrapped around the surface of oriented SF scaffolds to form a combined periosteum-diaphysis substitute (SFMC). Finally, SFMC grafts were implanted into segmental bone defects of rabbit radius for assessing the capacity of bone repair (Scheme 1).

2. Materials and Methods

2.1 Preparation of electrospun SF membranes

Silkworm cocoons (New Silk Road Ltd, China) (6-8 g) were degummed twice with 3 L of 0.4% Na_2CO_3 solution at 98 ºC for 40 min and then dissolved in 9.3 M LiBr (Sigma-Aldrich, USA) solution. The solution was dialyzed for 72 h (Viskase, MWCO 3500 Da). The SF solution was frozen overnight at -80 ºC and freeze-dried for 72 h. The lyophilized

SF was dissolved in hexafluoroisopropanol for electrospinning. The flow rate, voltage, and distance from the nozzle to the collection device were set as 1 mL/h, 12 kV, and 10 cm, respectively. Electrospun SF membranes were dried overnight at room temperature to evaporate residual solvent.

2.2 Preparation of biomimetic periosteum-diaphysis substitutes

The biomimetic periosteum-diaphysis substitute was prepared by wrapping an electrospun SF membrane on a tubular SF scaffold. The tubular SF scaffold with oriented and interconnected pores was fabricated by directional freeze-drying. In brief, the SF solution was added into silicone molds and frozen by liquid nitrogen. SF scaffolds were then collected from the silicone molds, treated with 90% methanol for 30 min to induce the formation of β-sheet structures rendering them insoluble in aqueous solutions. Electrospun SF membranes were wrapped around SF tubular scaffolds to form the biomimetic periosteum-diaphysis substitutes.

2.3 Characterizations of biomimetic periosteum-diaphysis substitutes

The morphology of electrospun SF membranes and biomimetic periosteum-diaphysis substitutes was observed by scanning electron microscopy (SEM, S-4800, Hitachi, Kyoto, Japan). The hydrophilicity of electrospun membranes was analyzed using a contact angle tester (Kruss, Germany). The mechanical properties of electrospun SF membranes were determined using a universal testing machine (HY-0580, Shanghai Hengyi Co., Ltd, China). The tensile modulus of the membranes was calculated according to the stress-strain curve.

In vitro degradation of biomimetic periosteum-diaphysis substitutes was evaluated by monitoring the weight loss. The initial weight of SF composite scaffolds was recorded under absolute dry conditions. Then the scaffolds were placed in PBS solution on a thermostatic oscillator at 37 ºC. The samples were collected (0, 10, 20, 30, 40, 50 and 60 days), dried at 55 ºC, and weighed to calculate weight loss.

2.4 Cell proliferation on SF electrospun membranes

Prior to cell culture, SF membranes were placed on glass coverslips (Φ 14 mm), sterilized with 75% ethanol for 30 min, and then soaked overnight in culture medium (Gibco). To test the biocompatibility of the membranes, BMSCs and EPCs were co-cultured at the ratio of 1:0, 0:1, 2:1, 1:1 and 1:2 at a density of 10^4 cells (BMSCs + EPCs)/cm^2. Cells were cocultured in a 1:1 mixture of α-MEM medium (Gibco) and endothelial growth medium-2 (EGM-2, Lonza Inc) at 37 ºC in 5% CO_2. Cell proliferation was assessed using the cell counting kit-8 reagent (CCK-8, Beyotime, Haimen, China) on days 1, 3, and 5.

BMSCs and EPCs were labeled with Dil (green, Beyotime) and Dio (red, Beyotime) dyes, respectively. Labeled cells were seeded on the membranes at the ratios described above. On days 1, 3, and 5 of the incubation period the cells were observed with a fluorescence microscope (Carl Zeiss Inc, Thornwood, NY, USA). Cell morphology was also observed by SEM.

2.5 Evaluation of *in vitro* osteogenesis

2.5.1 ALP and AR staining

The BMSCs and EPCs were seeded on membranes as described above and co-cultured at the ratio of 1:0, 2:1, 1:1 and 1:2. Cell culture of 1:0, 2:1, 1:1 and 1:2 groups was carried out in 1:1 mixture of osteogenic differentiation medium (supplemented with 10% FBS, 1% penicillin/streptomycin, 0.1 μmol/L dexamethasone, 10 mmol/L β-glycerol phosphate, and 50 μmol/L ascorbate) and endothelial growth medium-2 at 37 ºC in 5% CO_2. In control group, BMSCs were cultured with α-MEM medium containing 10 % fetal bovine serum and 1 % penicillin-streptomycin.

After osteogenic induction for 7 days, cells were stained with an alkaline phosphatase (ALP) staining kit (Cyagen, Guangzhou, China). Images of ALP staining were captured using an optical microscope (Zeiss). On day 14 of osteogenic induction, the recommended amount of pre-prepared 0.1% alizarin red (AR) staining solution (Cyagen, Guangzhou, China) was added and incubated for 20 min. After three washes in PBS, images of the red-stained calcareous nodules were taken using an optical microscope (Zeiss).

2.5.2 qRT-PCR

At 7 days and 14 days of osteogenic induction, quantitative real-time polymerase chain reaction (qRT-PCR) was performed to detect the expression of the osteogenic genes *COL1A1*, *ALPL*, *RUNX2,* and *BGLAP*. Total RNA was extracted using RNA isolater Total RNA Extraction Reagent (Vazyme Biotech Co.,Ltd, Jiangsu, China) and complementary DNA (cDNA) was synthesized using the cDNA kit (Thermo Fisher Scientific). PCR amplification was performed in a CFX96 TM Real-Time PCR System instrument using

the iTap TM Universal SYBR Green Supermix. Relative expression of target genes was calculated as follows: $\chi=2^{-\Delta\Delta CT}$. The primer sequences are listed in Table 1.

2.5.3 Western blot

Radio immunoprecipitation assay lysis buffer (RIPA, Beyotime) containing protease inhibitors was used to extract cellular proteins. The protein concentration was determined using a BCA kit (Absin Bioscience Inc., abs9232 Shanghai, China). After blocking for 1 h, the membranes were incubated overnight at 4 ºC with the desired antibodies (Abcam, anti-collagen I: ab34710, anti-osteocalcin: ab93876, anti-α-Tubulin: ab7291, anti-ALP: ab229126, anti-RUNX2: ab192256, anti-VEGF: ab46154). The following day the membranes were incubated with horseradish peroxidase (HRP) labeled secondary antibodies (ab6721 or ab6788) for 1 h. The hypersensitive chemiluminescence substrate (Beyotime) was added to the membrane for visualization. The optical density (OD) value was analyzed by ImageJ software (National Institutes of Health, USA) with α-Tubulin serving as control for the standardization of protein content.

2.5.4 Immunofluorescence

After 7 and 14 days of osteogenic induction, the cells were fixed and immersed in blocking buffer. The cell membranes were permeabilized by 0.1% Triton X-100 for 10 min and the cells were incubated in the desired diluted antibodies (anti-collagen I, ab34710, anti-CD31, ab28364) for 8 h at 4 ºC. Then the cells were incubated with an Alexa Fluor conjugated secondary antibody (ab150075) mixed with phalloidin (C1033,

Beyotime) for 1 h. Nuclei were counterstained using 4',6-diamidino-2-phenylindole (DAPI, Beyotime). Images were captured using a fluorescence microscope.

2.6 Evaluation of *in vitro* angiogenesis by the co-cultured cells

The BMSCs and EPCs were seeded on the membranes as described above and co-cultured at the ratio of 1:0, 2:1, 1:1 and 1:2. Cell culture of 1:0, 2:1, 1:1 and 1:2 groups was carried out in 1:1 mixture of endothelial growth medium-2 (supplemented with 2% FBS and growth factors, including 50 ng/ml VEGF, 1 ng/ml basic fibroblast growth factor and 2 ng/ml insulin-like growth factor 1) and α-MEM medium at 37 ºC in 5% CO_2. In control group, BMSCs were cultured with α-MEM medium containing 10 % fetal bovine serum and 1 % penicillin-streptomycin.

At 3 and 5 days of culture, qRT-PCR and Western blot analysis were performed to detect the expression of vascular endothelial growth factor (VEGF). The expression of CD31, a vascular marker protein, was detected by immunofluorescence. The experimental steps were performed as described in section 2.4 above. The genes and corresponding primers are listed in Table 1.

2.7 Animal studies

BMSCs and EPCs (1:1) were co-cultured on electrospun SF membranes for 7 days to form a biomimetic periosteum. On the 7^{th} day the cell-laden membranes were wrapped around the SF tubular scaffolds to form the biomimetic periosteum-diaphysis substitutes for the subsequent animal experiments. Biomimetic periosteum-diaphysis substitutes without cells were also prepared for the control.

New Zealand white rabbits (6 weeks) were used in the animal experiments. All surgical procedures were approved by the Soochow University Laboratory Animal Management Committee. All *in vivo* animal experiments were performed according to previously described experimental protocols [25-27, 38]. Feeding and drinking water were prohibited 12 hours before surgery. The rabbits were anesthetized with 4% isoflurane and 30% oxygen. The rabbit was placed in a lateral position, and the left upper limb was prepared with skin and sterile drapes. First, the operative limb was is wrapped with a tourniquet and a 4 cm longitudinal incision was made in the posterior middle of the forearm. The skin, fascia and muscle were cut open in turn until the exposure the radius. A critical-size bone defect model was prepared by removing a 15 mm bone block using a miniature chainsaw. Twenty-four rabbits were randomly divided into four groups. The rabbits in the control group had bilateral radius defects without implants. In the SF group, tubular SF scaffolds were implanted into the defects. In the SFM group, the defects were implanted with cell-free periosteum-bone substitutes. Finally, animals in the SFMC group received the implantation of cell-laden periosteum-bone substitutes. The fascia and skin were sutured, and the wound was bandaged. Feeding and drinking were resumed 6 hours after operation, and the rabbits were kept in separate cages. Intramuscular penicillin (5 mg/kg) was performed for 3 days after operation to prevent infection.

2.8 Micro-CT

Rabbits were euthanized at 6 or 12 weeks. Radius specimens were harvested for gross observation and fixed with 10% formalin (Aladdin). All samples were scanned

using a Micro-CT (SkyScan, Aartselaar, Belgium). Data reconstruction was performed using NRecon software (Skyscan) to generate 2D and 3D images. Image analysis was performed using the CTAn software (Skyscan). The volume of interest in bone regeneration was defined as the cylindrical area covering the initial bone defect and the bone volume to tissue volume ratio (BV/ TV, %) was calculated.

2.9 Histology and immunohistochemistry

The samples were decalcified in 14% ethylene diamine tetraacetic acid (EDTA, Aladdin) for 2 months. After the decalcification was complete, the bones were paraffin embedded, sectioned, deparaffinized with xylene for 20 min, and dehydrated in alcohol for 10 min. For histologic observations, sections were stained with hematoxylin and eosin (H&E). For immunohistochemical staining, sections were blocked with 1% bovine serum albumin (Aladdin) after an incubation in 2 mg/mL hyaluronidase (Aladdin). The sections were incubated with an anti-COL I (Abcam, ab34710) or anti-CD31 (Abcam, ab28364) antibody overnight at 4 ºC. Subsequently, the sections were incubated with HRP-conjugated goat anti-rabbit secondary antibody (Abcam, ab6721) and visualized using 3,3′-diaminobenzidine solution (Vector Laboratories, Germany). The percentage of positive cells was quantitatively evaluated using ImageJ software.

2.10 Statistical analysis

The experimental results were statistically analyzed using the SPSS 19.0 and Sigma Plot 14.0 software packages. Results were expressed as mean ± standard deviation. Comparisons between two groups were performed with independent two-tailed Student's

t-test while comparisons between multiple groups were conducted using one-way Analysis of Variance (ANOVA) followed by Tukey's post hoc test. A p value of less than 0.05 was considered statistically significant.

3. Results

3.1 The structure of biomimetic periosteum-diaphysis substitutes

The biomimetic periosteum-diaphysis substitute was composed of an electrospun SF membrane and a tubular SF scaffold, as shown in Figure 1A, B, C, F. The electrospun membrane acted as the biomimetic periosteum. The surface morphology of these membranes was observed via SEM. The average fiber diameter was 0.6 ± 0.13 μm (Figure S1). Water contact angle of the membrane was 42.0 ± 1.2º (Figure 1D), indicating that the substrate was hydrophilic, which is benificial for cell growth and nutrient transport. The stress–strain curve of electrospun SF membranes (Figure 1E) showed that the membrane was elastic, and its tensile strength and maximum strain were 1.5 MPa and 15%, respectively.

To support the artificial periosteum and promote bone regeneration, an SF tubular scaffold with directionally connected pores was utilized as biomimetic diaphysis (Figure 1F). The pores of these tubular scaffolds were oriented with pore diameters ranging from 20 to 100 μm and a porosity of approximately 60%. It was reported that the minimum pore size necessary for significant bone growth was 75-100 μm [28], while the micropores could facilitate the exchange of nutrients, oxygen, and the transport of waste.

Subsequently, electrospun SF membranes were wrapped on the surface of SF tubular scaffolds to form combined periosteum-bone substitute. Obtained SEM images clearly showed the membrane layer and the hollow scaffold structure. Photographs of the scaffold further illustrated the tubular structure (Figure 1G). *In vitro* degradation assays showed that 40% of SF was partially degraded within 2 months (Figure 1H).

3.2 *In vitro* biocompatibility of electrospun SF membranes

To evaluate the effect of electrospun SF membranes on the proliferation of co-cultured cells, BMSCs and EPCs were seeded on the membranes for 1, 3 and 5 days at different ratios (1:0, 0:1, 2:1, 1:1 and 1:2). Cell proliferation assays were performed using cell tracking (Figure 2A) and the CCK-8 cell proliferation assay (Figure 2C). The results showed that both BMSCs (green) and EPCs (red) grew well on the membranes. The number of both cells increased significantly, and there was no significant difference between the proliferation of the two different cell populations (Figure 2A, C). The morphology of cells on the SF membranes was also determined by SEM. As shown in Figure 2B, cells spread well on the nanofibers at 3 days. These results indicated the excellent biocompatibility of electrospun SF membranes that were able to support the proliferation of co-cultured cells.

3.3 *In vitro* osteogenesis by co-cultured cells on electrospun SF membranes

To evaluate the osteogenic potential of co-cultured BMSCs and EPCs on electrospun SF membranes, the cells were stained to detect the expression of ALP. The expression of genes and proteins involved in osteogenic differentiation was quantitated, and the

deposition of calcium crystals was also visualized. The results showed that the expression of ALP in co-cultured cells (2: 1, 1: 1, 1: 2) was much higher compared to monoculture. The expression of ALP at a 1:1 BMSC to EPC ratio was significantly up-regulated (Figure 3A, C). AR staining showed abundant calcium deposits after 14 d in culture at 1:1 cell ratio. Calcium nodules were also seen in other co-culture groups but their intensity was lower (Figure 3B, D). The results of qRT-PCR and Western blot analyses showed that the expression of osteogenic gene transcripts (*ALPL, RUNX2, COL1A1, BGLAP*) and proteins (ALP, Runx2, COL I, and OCN) were significantly upregulated at 1:1 cell ratio (Figure 4). In addition, immunofluorescence images clearly demonstrated the expression of collagen I (COL I). These results demonstrated that the co-culture of BMSCs and EPCs at a ratio of 1:1 provided optimal conditions to induce osteogenic differentiation of stem cells (Figure 5). In summary, we found that the co-culture of BMSCs and EPCs could promote the osteogenic differentiation of BMSCs, and the optimal BMSC to EPC ratio was 1:1.

3.4 *In vitro* angiogenesis ability of BMSCs and EPCs co-cultured on the electrospun SF membranes

VEGF and CD31 are markers of early angiogenesis, the *in vitro* expression of VEGF and CD31 was detected at different time points, such as 3, 4, 5, 6 and 7 days [29-32]. In this experiment, we intended to evaluate angiogenesis in early time, and then in vitro expression of VEGF and CD31 at 3 and 5 days was detected. The results showed the upregulated expression of angiogenic genes and proteins in co-cultured cells at a ratio of

2:1, 1:1 and 1:2. The results of qRT-PCR and Western blot showed that VEGF was significantly upregulated both at mRNA and protein level in co-cultures at 1:2 cell ratio, followed by the 1:1 group, the 2:1 group, the 1:0 group and the Control group (Figure 6). The expression of CD31 was detected visually by immunofluorescence (Figure 7). The immunofluorescent staining showed that culturing cells at a 1:2 ratio resulted in the most pronounced CD31 expression, followed by the 1:1 group, the 2:1 group, the 1:0 group and the Control group. These results suggested that that culturing BMSCs and EPCs at a ratio of 1:2 resulted in more *in vitro* angiogenic changes, followed by the 1:1, 2:1, 1:0, and the Control group.

3.5 Repair of segmental bone defects in rabbit radius using the biomimetic periosteum-diaphysis substitutes

Cell-laden periosteum-diaphysis substitutes were used to repair large segmental bone defects in the radius of rabbits. To prepare the cell-loaded periosteum-diaphysis substitutes, BMSCs and EPCs were incubated at a ratio of 1:1 on electrospun SF membranes for 7 days. The implantation of the biomimetic bone grafts was carried out as described in section 2.6. The samples were harvested at 6 and 12 weeks after surgery. On gross visual inspection, only a small amount of new bone formed in the control group at 6 weeks (Figure 8A). In comparison, the groups implanted with various forms of bone substitutes exhibited better healing tendencies, with animals in the SFMC group showing the most extensive repair. After 12 weeks, the bone defects in the control group were still clearly obvious, while the defects were almost completely filled with new bone in animals

368 receiving implanted scaffolds. Consistently, the SFMC group showed the best healing
369 results by gross observation.

370 The quality of the newly formed bone was analyzed by micro-CT (Figure 8B). In
371 control animals, the bone defects were still apparent at 6 weeks after the initial bone loss.
372 Newly formed bone was evident in the SF, SFM, and SFMC groups, connecting the
373 proximal and distal ends of the radius defect. Interestingly, the formation of medullary
374 cavity-like structures was already visible at this time point in the SFMC group.
375 Regenerating bones in the other groups did not show this feature. In addition, the SFMC
376 group showed more new bone formation than other groups. However, the morphology of
377 the new bone remained significantly different from that of a non-injured radius. At 12
378 weeks, the bone volume to tissue volume ratio (BV/TV) doubled (Figure 8C). The best
379 bone repair was seen in the SFMC group where BV/TV reached more than 70%. These
380 observations clearly indicated that superior bone healing in animals receiving cell-laden
381 SF-based biomimetic periosteum-diaphysis substitutes. In this group, segmental bone
382 defects healed significantly better and medullary cavities were formed, to mimick the
383 natural structure of long bone.

384 Sections of newly formed bone segments were also observed microscopically using
385 H&E staining (Figure 9A, C). As expected, there was very little evidence of bone repair
386 in the control group at 6 weeks. In contrast, in the SF, SFM, and SFMC groups a
387 significant amount of new bone matrix was visible in the area of the initial defect. New
388 bone formation increased significantly by 12 weeks. Again, noticeably less bone

formation was evident in the control group. In contrast, in the SFMC group, a clear bone marrow cavity formed and myeloid tissue started to enter into this space. These results underline the fact that large segmental bone defects have a very limited capacity to heal spontaneously. The amount of new bone increased in the SF group but the new bone was growing into the inserted grafts from the two ends towards the middle. These results indicated that the oriented tubular SF scaffolds could connect the broken ends and promoted nutrient circulation, resulting in some repair. Bone regeneration and remodeling was much faster and efficient in the SFMC group, where the forming new bone showed some remarkable similarity to normal bone. These findings clearly supported that importance of the BMSCs and EPCs in promoting osteogenesis. In summary, these results showed that the biomimetic periosteum-diaphysis substitute formed by the culturing of BMSCs and EPCs onto electrospun SF membranes combined with a degradable SF tubular scaffold demonstrated a remarkable potential to promote the repair of large segmental bone defects.

The expression of osteogenic markers was also investigated in the freshly formed bone segments using immunohistochemistry (Figure 9B, D). The expression of COL I increased in all groups at 6 and 12 weeks after implantation, with the highest expression levels in the SFMC group. In conclusion, the results showed that the biomimetic periosteum-diaphysis substitute could promote the expression of bone-related matrix proteins, with the amount of expression increasing during longer implantation times. Thus,

409 the biomimetic periosteum-diaphysis substitute had the potential to promote osteogenesis
410 and the repair of large segmental bone defects.

411

412 **4. Discussion**

413 The periosteum, a fibrous tissue covering the surface of all bones, is the natural
414 source of pluripotent progenitor cells that mediate the repair of fractured bones [33]. In
415 1739, Duhamel noted that the function of the deep layer of the periosteum was similar to
416 that of the cambium layer of trees and named it accordingly [34]. The periosteum consists
417 of two distinct layers. The outer fibrous layer is mainly composed of fibroblasts
418 embedded in collagen fibers. In contrast, the inner cambium layer is the source of cells
419 and growth factors necessary for bone repair. In addition, the periosteum also contains a
420 network of arteries and veins forming a dense reticular vascular layer around bones.
421 During the process of bone regeneration, the cambium layer provides a variety of stem
422 cells, cytokines, and growth factors. The characteristic of cambium layer composition is
423 vital for bone regeneration, and it can accelerate bone formation by promoting
424 endochondral and intramembranous ossification [35, 36]. Several studies have shown that
425 the lack of periosteum resulted in the nonunion or malunion, while autologous periosteum
426 transplantation could promote bone healing [37].

427 Given the indispensable role of periosteum, extensive attempts have been made to
428 create tissue-engineered substitutes to facilitate the regeneration of injured bone tissue.
429 While early work focused primarily on providing a replacement for the physical structures
430 of the periosteum, more advanced biomimetic periosteum, containing cellular
431 components, showed clear advantages by supporting osteogenesis and angiogenesis.

These biomimetic grafs were comparable to the native periosteum both in cellular composition and function. However, the application of cell-based biomimetic periosteum is limited by unsatisfactory tensile properties and restrictive storage requirements [38]. Artificial periosteum transplanted into bone defects is exposed to forces created by the movements of fractured bone ends. Once the artificial periosteum is broken, the benefits become limited.

In this study, we prepared a biomimetic periosteum replicating the key features of the natural cambium layer. To achieve this, BMSCs and EPCs were seeded onto electrospun SF membranes. This approach improved the mechanical properties of the artificial mimics, while recreating the microstructure of natural periosteum. Natural ECM provides a surface for cellular growth and enhances cell differentiation and maturation . SF has good biocompatibility and low immunogenicity [39]. Furthermore, compared with collagen, SF membranes had better mechanical properties and longer degradation time. Low-cost production and ease of use make SF an ideal biomaterial for the preparation of biomimetic periosteum. Previous studies used various polymers, including polylactic acid and polycaprolactone to replace the ECM [40]. Although these polymers possessed satisfying mechanical properties, the drugs and/or growth factors needed to be encapsulated in them to improve their biological characteristics. Often these molecules had burst release in the early stage, causing anomalous cell behavior and unpredictable side effects. In addition, in these versions of artificial periosteum, endogenous scaffolds were limited to the use of cell-sheets and acellular scaffolds due to issues with biocompatibility and immunogenicity [41]. However, the use of such scaffolds was found to be limited by unsatisfactory mechanical properties and rapid degradation. In our study, we combined the advantages of artificial polymer membranes and endogenous scaffolds

by seeding BMSCs and EPCs onto an SF membrane. The created biomimetic periosteum, assembled on an electrospun SF membrane, retained the advantages of natural ECM, had excellent mechanical properties, and a slow degradation rate. Moreover, we achieved the long-term release of osteogenic and angiogenic growth factors by loading BMSCs and EPCs onto the membrane. The use of electrospun SF membranes loaded with BMSCs and EPCs appears to be a promising strategy for the development of a biomimetic periosteum.

The process of bone remodeling includes the differentiation of BMSCs, and angiogenesis induced by EPCs. BMSCs that are indispensable stem cells in the formation and differentiation of osteoblast at the implant-bone interface. BMSCs transplanted into bone defects promoted bone regeneration through proliferation, migration, osteogenic differentiation, and calcium deposition. In addition, BMSCs can also contribute to accelerated angiogenesis by endogenous EPCs though paracrine secretory pathways [42]. Through this mechanism they secrete proangiogenic cytokines, such as VEGF-A, thus promoting the differentiation and homing of EPCs, and the repair of injured endothelial cells [43]. The recruitment of EPCs has been shown to significantly promote neovascularization [44]. Many studies have found that BMSC and EPC interact by secreting various growth factors such as VEGF and platelet derived growth factor (PDGF) [45]. BMSC could also reduce EPC apoptosis through direct cell-cell contact. Liang et al. found that co-culture of BMSC and EPC enhanced PDGF secretion and angiogenesis [46]. Aguirre et al. reported that BMSCs and EPCs jointly promote the formation of tubular structures in a co-culture system [47]. Differentiating EPCs also secrete BMP-2, one of the most powerful osteogenesis-promoting cytokines. BMPs accelerate osteogenesis and angiogenesis simultaneously, while reducing the occurrence of complications during

bone remolding [48]. Furthermore, it was reported that directional mitochondrial exchange occurred between MSCs and vascular endothelial cells via intercellular tunneling nanotubes (TNT) [49]. This TNT-mediated mitochondrial transfer has the potential to protect injured vascular endothelial cells from mitochondrial dysfunction, by increasing mitochondrial membrane potential, inhibiting the excessive accumulation of reactive oxygen species, and the reconstitution of mitochondrial respiration [50].

Previous studies have shown that the co-culture of BMSCs and EPCs can promote osteogenesis and angiogenesis. He et al. reported that the optimal ratio of BMSCs and EPCs in osteogenic differentiation was 1:1, with the highest ALP activity occurring at this ratio [51]. In contrast, Peng et al. found that the optimal BMSC to EPC ratio for angiogenesis and osteogenesis was 1:3 and 2:1, respectively [52]. Fu et al. also studied the behavior of EPCs and BMSCs in co-cultures [53]. They found that increasing the proportion of EPCs promoted the expression of CD31 and improved the vascularization of scaffolds. The expression of osteogenic and angiogenic markers was the highest when the EPC to BMSC ratio was 3:1. In our study, co-culturing BMSCs and EPCs at a ratio of 1:1 showed the most effective in both osteogenesis and angiogenesis. Therefore, we used BMSCs and EPCs at this ratio to prepare biomimetic periosteum to replicate the ability of natural cambium layer to promote bone regeneration.

Nonunion is a potentially catastrophic complication of long segmental bone fractures. Ensuring adequate mechanical support is a critical requirement in the treatment of these defects. To achieve this aim, we designed a hollow tubular scaffold with oriented connected pores mimicking the porous structure and oriented collagen fibers of native long bones. Studies have shown that compared to randomly porous scaffolds, alternatives with directional porous structure were more conducive to the migration of cells, the

exchange of nutrients and the deposition of ECM [54]. Currently, 3D printing and directional freeze-drying represent the most promising technologies to prepare directionally porous scaffolds. However, 3D printing is not suitable for water-soluble materials while freeze-drying shows superior versatility and cost. Therefore, we utilized directional freeze-drying to prepare hollow tubular scaffolds containing oriented and connected pores to fill the space between the ends of broken bones. The connected pores in these structures facilitate the migration and deposition of osteoblasts in the bone matrix [55]. The importance of anatomic reduction and stable fixation in the healing of bone fractures has long been recognized [56]. Hollow tubular scaffolds can provide mechanical support, helping to fix the long axis of the broken ends along natural force lines. It is important to note that the implantation of scaffolds can prevent soft tissues from occupying bone defects [57], thus reducing the risk of bone nonunion. Therefore, the combination of hollow tubular scaffolds with biomimetic periosteum represents an ideal combination in promoting bone regeneration.

Various studies have reported the application of biomimetic periosteal substitutes. For example, some studies have combined artificial periosteum and allogeneic bone to form periosteal bone substitute, but the defect of allogeneic bone graft is inevitable [58, 59]. In addition, there are some studies combined artificial periosteum and artificial bone scaffold [38], but these scaffolds have no directional pores and interconnected pores, which is not conducive to the transport of nutrients, air and metabolic waste. Our approach differs in three respects. First, we offset the disadvantages of the poor mechanical properties of ECM sheets by seeding cells on easily prepared and strong SF membranes. Second, we verified that the optimal ratio of BMSCs and EPCs was 1:1. The SF membranes loaded with the combination of stem cells could act as a source of

bioactive factors over a longer period of time, promoting angiogenesis and bone regeneration. Finally, instead of using a biomimetic periosteum alone, hollow tubular scaffolds were introduced as a support and space holder. The resulting biomimetic periosteum-diaphysis substitutes act as an artificial diaphysis in promoting the regeneration of critical-sized segmental bone defects. The observed medullary cavity formation in the SFMC treatment group suggests that this approach represents a promising novel method for supporting bone regeneration.

5. Conclusion

We developed a biomimetic periosteum-diaphysis substitute by integrating the biomimetic cambium layer, fabricated by seeding BMSCs and EPCs on an electrospun SF membrane, with a tubular SF scaffold. The biomimetic periosteum had an ECM-like microstructure, supporting the proliferation of BMSCs and EPCs and promoting osteogenesis and angiogenesis. We found that in the construction of biomimetic periosteum, the optimal ratio of BMSCs and EPCs was 1:1. The SF hollow tubular scaffold, which acts as biomimetic diaphysis substitute, contains oriented interconnected pores. Finally, animal experiments demonstrated that the biomimetic periosteum-diaphysis graft was extremely effective in promoting bone regeneration. Furthermore, the formation of connected medullary cavities inside these scaffolds even promoted the return of bone marrow-like cellular composition. These findings clearly demonstrated that the developed biomimetic periosteum-diaphysis substitute represents a promising approach

for the repair of large segmental bone defects, paving the way to provide a novel strategy for the replacement of large missing bone segments.

Author statement

Lili Yu: Conceptualization, Methodology, Validation, Formal analysis, Investigation, Data curation, Writing - original draft, Writing - review & editing, Visualization. Qiang Wei: Validation, Formal analysis, Investigation, Writing - review & editing. Jiaying Li: Methodology, Formal analysis, Writing - review & editing. Huan Wang: Methodology, Formal analysis, Data curation. Qingchen Meng: Investigation, Data curation. En Xie: Investigation, Data curation. Zexi Li: Methodology, Formal analysis. Kexin Li: Methodology. Wenmiao Will Shu: Methodology, Writing - review & editing. Junxi Wu: Methodology. Lei Yang: Methodology. Yan Cai: Conceptualization, Methodology, Writing - review & editing. Fengxuan Han: Conceptualization, Formal analysis, Funding acquisition, Writing - review & editing. Bin Li: Conceptualization, Writing - review & editing, Visualization, Supervision, Project administration, Funding acquisition.

Data and materials availability

All data are available in the main text.

Declaration of competing interest

The authors declare that they have no known competing financial interests or personal relationships that could have appeared to influence the work reported in this paper.

Acknowledgments

The authors are grateful for the funding provided for this study by the National Key Research and Development Program of China (2020YFC1107401), the National Natural Science Foundation of China (81925027, 82111530157, 31872748), the Royal Society (IEC\NSFC\201166), Jiangsu Provincial Special Program of Medical Science (BL2012004), and the Priority Academic Program Development (PAPD) of Jiangsu Higher Education Institutions.

References

[1] Witek L, Alifarag AM, Tovar N, Lopez CD, Cronstein BN, Rodriguez ED, et al. Repair of critical-sized long bone defects using dipyridamole-augmented 3D-printed bioactive ceramic scaffolds. J Orthop Res 2019; 37: 2499-2507.

[2] Bornert F, Clauss F, Hua GQ, Idoux-Gillet Y, Keller L, De Grado GF, et al. Mechanistic illustration: How newly-formed blood vessels stopped by the mineral blocks of bone substitutes can be avoided by using innovative combined therapeutics. Biomedicines 2021; 9: 952.

[3] Wu L, Gu Y, Liu L, Tang J, Mao J, Xi K, et al. Hierarchical micro/nanofibrous membranes of sustained releasing VEGF for periosteal regeneration. Biomaterials 2020; 227: 119555.

[4] Wieding J, Lindner T, Bergschmidt P, Bader R. Biomechanical stability of novel mechanically adapted open-porous titanium scaffolds in metatarsal bone defects of sheep. Biomaterials 2015; 46: 35-47.

[5] Zhang M, Matinlinna J, Tsoi J, Liu W, Cui X, Lu W, et al. Recent developments in biomaterials for long-bone segmental defect reconstruction: A narrative overview. J Orthop Transl 2020; 22: 26-33.

[6] Zhou Y, Han S, Xiao L, Han P, Wang S, He J, et al. Accelerated host angiogenesis and immune responses by ion release from mesoporous bioactive glass. J Mater Chem B 2018; 6: 3274-3284.

[7] Zhang X, Awad H, O'Keefe R, Guldberg R, Schwarz E. A perspective: engineering periosteum for structural bone graft healing. Clin Orthop Relat R 2008; 466: 1777-1787.
[8] Sun YG, Gao ZW, Zhang XP, Xu ZY, Zhang YH, He BB, et al. 3D-printed, bi-layer, biomimetic artificial periosteum for boosting bone regeneration. Bio-Des Manuf 2022; 5: 540-555.
[9] Cao S, Zhao Y, Hu Y, Zou L, Chen J. New perspectives: In-situ tissue engineering for bone repair scaffold. Compos B Eng 2020; 202: 108445.
[10] Kang F, Yi Q, Gu P, Dong Y, Zhang Z, Zhang L, Bai Y. Controlled growth factor delivery system with osteogenic-angiogenic coupling effect for bone regeneration. J Orthop Translat 2021; 31: 110-125.
[11] Cheng WX, Liu YZ, Meng XB, Zheng ZT, Li LL, Ke LQ, et al. PLGA/β-TCP composite scaffold incorporating cucurbitacin B promotes bone regeneration by inducing angiogenesis. J Orthop Translat 2021; 31: 41-51.
[12] Yang Z, Yang Z, Ding L, Zhang P, Liu C, Chen D, et al. Self-adhesive hydrogel biomimetic periosteum to promote critical-size bone defect repair via synergistic osteogenesis and angiogenesis. ACS Appl Mater Inter 2022; 14: 36395-36410.
[13] Weisbrod L, Arnold P, Leever J. Radiographic and CT evaluation of recombinant human bone morphogenetic protein-2-assisted cervical spinal interbody fusion. Clin Spine Surg 2019; 32: 71-79.
[14] Feng Q, Xu J, Zhang K, Yao H, Zheng N, Zheng L, et al. Dynamic and cell-infiltratable hydrogels as injectable carrier of therapeutic cells and drugs for treating challenging bone defects. ACS Cent Sci 2019; 5: 440-450.
[15] Li Z, Wang H, Zhang K, Yang B, Xie X, Yang Z, et al. Bisphosphonate-based hydrogel mediates biomimetic negative feedback regulation of osteoclastic activity to promote bone regeneration. Bioact Mater 2021; 13: 9-22.
[16] Chen L, Li L, Xing F, Peng J, Peng K, Wang Y, et al. Human urine-derived stem cells: Potential for cell-based therapy of cartilage defects. Stem Cells Int 2018; 2018: 1-14.
[17] Polymeri A, Giannobile WV, Kaigler D. Bone marrow stromal stem cells in tissue engineering and regenerative medicine. Horm Metab Res 2016; 48: 700-713.
[18] Lou Y, Wang H, Ye G, Li Y, Liu C, Yu M, Ying B. Periosteal tissue engineering: current developments and perspectives. Adv Healthc Mater 2021; 10: e2100215.
[19] Kundu B, Rajkhowa R, Kundu SC, Wang X. Silk fibroin biomaterials for tissue regenerations. Adv Drug Deliv Rev 2013; 65: 457-470.
[20] Yang Y, Xu T, Zhang Q, Piao Y, Bei HP, Zhao X. Biomimetic, stiff, and adhesive periosteum with osteogenic-angiogenic coupling effect for bone regeneration. Small 2021; 17: e2006598.
[21] Zhu J, Chen D, Du J, Chen X, Wang J, Zhang H, et al. Mechanical matching nanofibrous vascular scaffold with effective anticoagulation for vascular tissue engineering. Compos B Eng 2020; 186: 107788.
[22] Wu X, Liu Y, Li X, Wen P, Zhang Y, Long Y, et al. Preparation of aligned porous gelatin scaffolds by unidirectional freeze-drying method. Acta Biomater 2010; 6: 1167-1177.
[23] Lou Z, Han X, Liu J, Ma Q, Yan H, Yuan C, et al. Nano-Fe3O4/bamboo bundles/phenolic resin oriented recombination ternary composite with enhanced multiple functions. Compos B Eng 2021; 226: 109335.

[24] Jiang SJ, Wang MH, Wang ZY, Gao HL, Chen SM, Cong YH, et al. Radially porous nanocomposite scaffolds with enhanced capability for guiding bone regeneration in vivo. Adv Funct Mater 2022; 32: 2110931.
[25] Zhang H, Zhou Y, Yu N, Ma H, Wang K, Liu J, et al. Construction of vascularized tissue-engineered bone with polylysine-modified coral hydroxyapatite and a double cell-sheet complex to repair a large radius bone defect in rabbits. Acta Biomater 2019; 91: 82-98.
[26] Zha Y, Li Y, Lin T, Chen J, Zhang S, Wang J. Progenitor cell-derived exosomes endowed with VEGF plasmids enhance osteogenic induction and vascular remodeling in large segmental bone defects. Theranostics 2021; 11: 397-409.
[27] Zheng S, Zhong H, Cheng H, Li X, Zeng G, Chen T, et al. Engineering multifunctional hydrogel with osteogenic capacity for critical-size segmental bone defect repair. Front Bioeng Biotechnol 2022; 10: 899457.
[28] Murphy CM, Haugh MG, O'Brien FJ. The effect of mean pore size on cell attachment, proliferation and migration in collagen-glycosaminoglycan scaffolds for bone tissue engineering. Biomaterials 2010; 31: 461-466.
[29] Yang Z, Yang Z, Ding L, Zhang P, Liu C, Chen D, et al. Self-adhesive hydrogel biomimetic periosteum to promote critical-size bone defect repair via synergistic osteogenesis and angiogenesis. ACS Appl Mater Interfaces 2022; 14: 36395-36410.
[30] Parthiban SP, Athirasala A, Tahayeri A, Abdelmoniem R, George A, Bertassoni LE. BoneMA-synthesis and characterization of a methacrylated bone-derived hydrogel for bioprinting ofin-vitrovascularized tissue constructs. Biofabrication 2021; 13: 035031.
[31] Zhang H, Ma W, Ma H, Qin C, Chen J, Wu C. Spindle-like zinc silicate nanoparticles accelerating innervated and vascularized skin burn wound healing. Adv Healthc Mater 2022; 11: e2102359.
[32] Cui J, Yu X, Yu B, Yang X, Fu Z, Wan J, et al. Coaxially fabricated dual-drug loading electrospinning fibrous mat with programmed releasing behavior to boost vascularized bone regeneration. Adv Healthc Mater 2022; 11: e2200571.
[33] Lin X, Zhao C, Zhu P, Chen J, Yu H, Cai Y, et al. Periosteum extracellular-matrix-mediated acellular mineralization during bone formation. Adv Healthc Mater 2018; 7: 1700660.
[34] Bilkay U, Tokat C, Helvaci E, Ozek C, Zekioglu O, Onat T, et al. Osteogenic capacities of tibial and cranial periosteum: a biochemical and histologic study. J Craniofac Surg 2008; 19: 453-458.
[35] Zhao L, Zhao JL, Yu JJ, Sun R, Zhang XF, Hu SH. In vivo investigation of tissue-engineered periosteum for the repair of allogeneic critical size bone defects in rabbits. Regen Med 2017; 12: 353-364.
[36] Ho-Shui-Ling A, Bolander J, Rustom LE, Johnson AW, Luyten FP, Picart C. Bone regeneration strategies: Engineered scaffolds, bioactive molecules and stem cells current stage and future perspectives. Biomaterials 2018; 180: 143-162.
[37] Moore SR, Heu C, Yu NYC, Whan RM, Knothe UR, Milz S, et al. Translating periosteum's regenerative power: insights from quantitative analysis of tissue genesis with a periosteum substitute implant. Stem Cell Transl Med 2016; 5: 1739-1749.
[38] Yu Y, Wang Y, Zhang W, Wang H, Li J, Pan L, et al. Biomimetic periosteum-bone substitute composed of preosteoblast-derived matrix and hydrogel for large segmental bone defect repair. Acta Biomater 2020; 113: 317-327.

[39] Wang Q, Zhou S, Wang S, You R, Yan S, Zhang Q, et al. Bioactive silk fibroin scaffold with nanoarchitecture for wound healing. Compos B Eng 2021; 224: 109165.
[40] Han F, Hu Y, Li J, Gong J, Guo Q, Zhu C, et al. In situ silk fibroin-mediated crystal formation of octacalcium phosphate and its application in bone repair. Mat Sci Eng C-Mater 2019; 95: 1-10.
[41] Wei Q, Wang S, Han F, Wang H, Zhang W, Yu Q, et al. Cellular modulation by the mechanical cues from biomaterials for tissue engineering. Biomater Transl 2021; 2: 323-342.
[42] Lian M, Sun B, Han Y, Yu B, Xin W, Xu R, et al. A low-temperature-printed hierarchical porous sponge-like scaffold that promotes cell-material interaction and modulates paracrine activity of MSCs for vascularized bone regeneration. Biomaterials 2021; 274: 120841.
[43] Wang Z, Bao X, Hu J, Shen S, Xu G, Wu Y. Nicotinamide riboside enhances endothelial precursor cell function to promote refractory wound healing through mediating the Sirt1/AMPK pathway. Front Pharmacol 2021; 12: 671563.
[44] Deng Y, Jiang C, Li C, Li T, Peng M, Wang J, et al. 3D printed scaffolds of calcium silicate-doped β-TCP synergize with co-cultured endothelial and stromal cells to promote vascularization and bone formation. Sci Rep 2017; 7: 5588.
[45] Xu H, Wang C, Liu C, Peng Z, Li J, Jin Y, et al. Cotransplantation of mesenchymal stem cells and endothelial progenitor cells for treating steroid-induced osteonecrosis of the femoral head. Stem Cells Transl Med 2021; 10: 781-796.
[46] Liang T, Zhu L, Gao W, Gong M, Ren J, Yao H, et al. Coculture of endothelial progenitor cells and mesenchymal stem cells enhanced their proliferation and angiogenesis through PDGF and Notch signaling. FEBS Open Bio 2017; 7: 1722-1736.
[47] Khojasteh A, Fahimipour F, Jafarian M, Sharifi D, Jahangir S, Khayyatan F, et al. Bone engineering in dog mandible: coculturing mesenchymal stem cells with endothelial progenitor cells in a composite scaffold containing vascular endothelial growth factor. J Biomed Mater Res B Appl Biomater 2017; 105: 1767-1777.
[48] Fitzpatrick V, Martin-Moldes Z, Deck A, Torres-Sanchez R, Valat A, Cairns D, et al. Functionalized 3D-printed silk-hydroxyapatite scaffolds for enhanced bone regeneration with innervation and vascularization. Biomaterials 2021; 276: 120995.
[49] Mittal R, Karhu E, Wang JS, Delgado S, Zukerman R, Mittal J, et al. Cell communication by tunneling nanotubes: Implications in disease and therapeutic applications. J Cell Physiol 2019; 234: 1130-1146.
[50] Liu KM, Ji KQ, Guo L, Wu W, Lu HX, Shan PY, et al. Mesenchymal stem cells rescue injured endothelial cells in an in vitro ischemia-reperfusion model via tunneling nanotube like structure-mediated mitochondrial transfer. Microvasc Res 2014; 92: 10-18.
[51] He XN, Dziak R, Yuan X, Mao KY, Genco R, Swihart M, et al. BMP2 genetically engineered MSCs and EPCs promote vascularized bone regeneration in rat critical-sized calvarial bone defects. PLoS One 2013; 8: e60473.
[52] Peng J, Chen L, Peng K, Chen XW, Wu J, He ZY, et al. Bone marrow mesenchymal stem cells and endothelial progenitor cells co-culture enhances large segment bone defect repair. J Biomed Nanotechnol 2019; 15: 742-755.
[53] Fu WL, Xiang Z, Huang FG, Gu ZP, Yu XX, Cen SQ, et al. Coculture of peripheral blood-derived mesenchymal stem cells and endothelial progenitor cells on strontium-

doped calcium polyphosphate scaffolds to generate vascularized engineered bone. Tissue Eng Pt A 2015; 21: 948-959.
[54] Pan Q, Li Y, Xu J, Kang Y, Li Y, Wang B, et al. The effects of tubular structure on biomaterial aided bone regeneration in distraction osteogenesis. J Orthop Translat 2020; 25: 80-86.
[55] Steijvers E, Ghei A, Xia Z. Manufacturing artificial bone allografts: a perspective. Biomater Transl 2022; 3: 65-80.
[56] Fuse Y, Zenke Y, Okimoto N, Yoshioka T, Yamanaka Y, Kawasaki M, et al. Biomechanical comparison of lag screw and non-spiral blade fixation of a novel femoral trochanteric nail in an osteoporotic bone model. Sci Rep 2022; 12: 2045-2322.
[57] Yang T, Tamaddon M, Jiang L, Wang J, Liu Z, Liu Z, et al. Bilayered scaffold with 3D printed stiff subchondral bony compartment to provide constant mechanical support for long-term cartilage regeneration. J Orthop Translat 2021; 30: 112-121.
[58] Li Y, Hoffman MD, Benoit DSW. Matrix metalloproteinase (MMP)-degradable tissue engineered periosteum coordinates allograft healing via early stage recruitment and support of host neurovasculature. Biomaterials 2021; 268: 120535.
[59] Romero R, Chubb L, Travers JK, Gonzales TR, Ehrhart NP, Kipper MJ. Coating cortical bone allografts with periosteum-mimetic scaffolds made of chitosan, trimethyl chitosan, and heparin. Carbohydr Polym 2015; 122: 144-151.

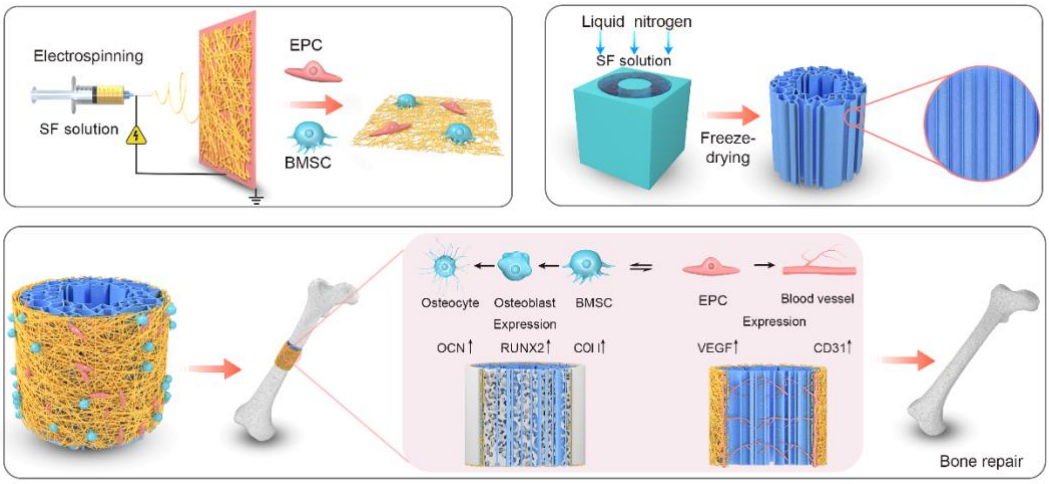

765

766 **Scheme 1**. Schematic illustration of the preparation and evaluating of a biomimetic

767 periosteum-diaphysis substitute composed of cell-loaded SF nanofibers and an oriented

768 SF scaffold for repair of large segmental bone defect.

769

770

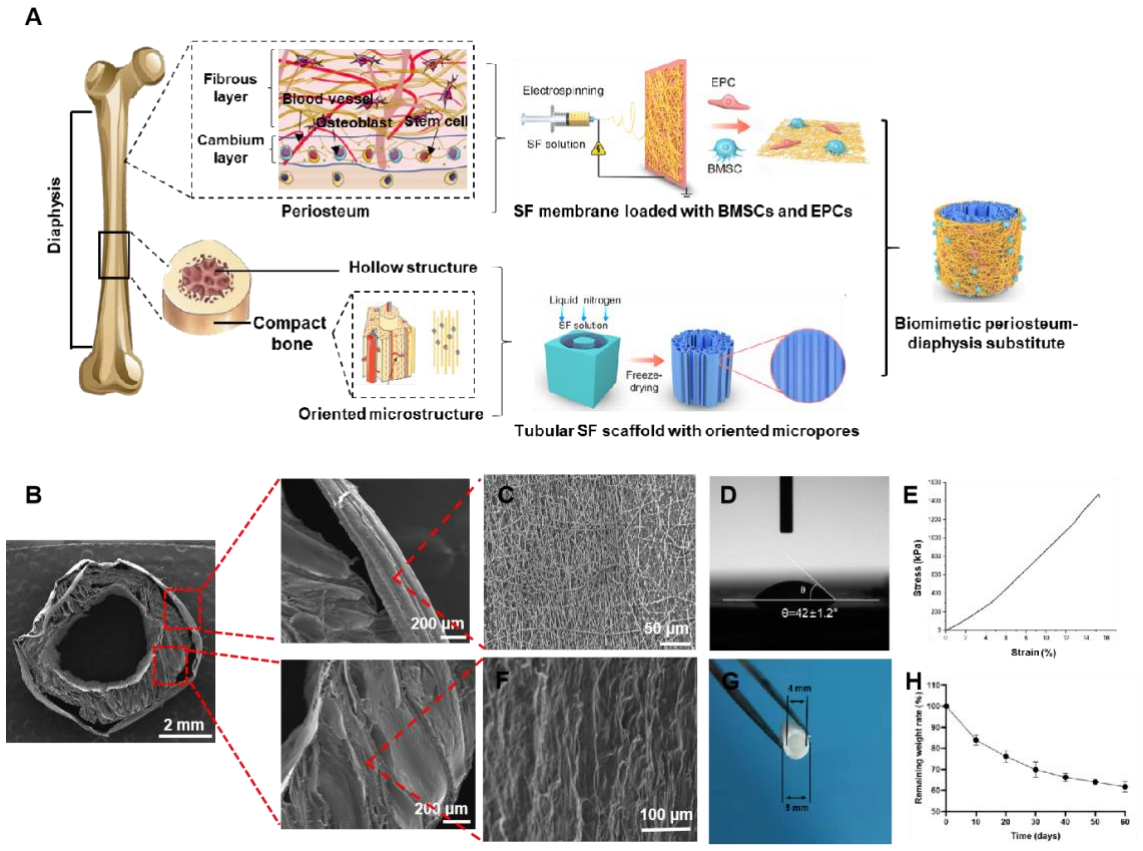

Figure 1. Characterizations of the biomimetic periosteum-bone substitute. (A) Illustration of structure and preparation of the biomimetic periosteum-bone substitute. (B) SEM images of the biomimetic periosteum-bone substitute, in which the electrospun SF membrane was wrapped around the SF scaffold. (C) SEM images of the electrospun SF membranes. (D) Water contact angle measurements (n=3). (E) Typical stress-strain curve of an electrospun SF membrane (n=3). (F) SEM images of the tubular SF scaffold. (G) Photographs of the tubular scaffold. (H) Degradation rate of the composite scaffolds (n=3).

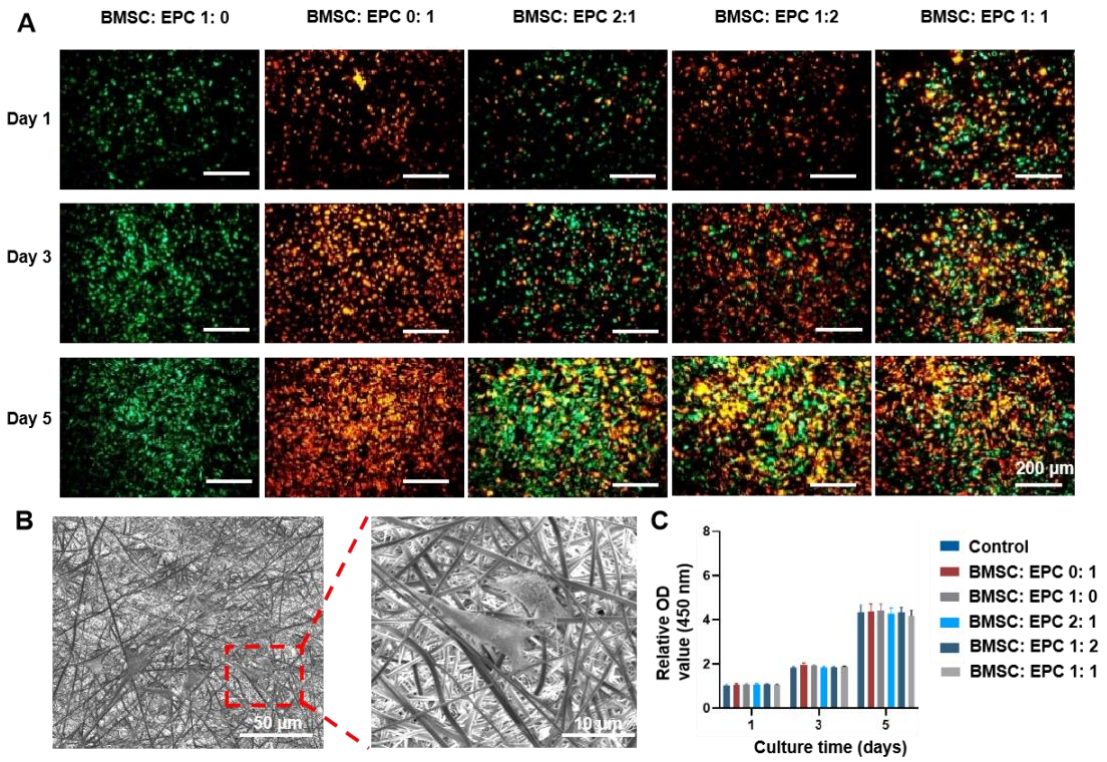

Figure 2. Cytocompatibility of electrospun SF membranes. (A) Cell tracking of different ratios of BMSCs (green) and EPCs (red) co-cultured on electrospun membranes at 1, 3 and 5 days. (B) SEM images of co-cultured BMSCs and EPCs on electrospun membranes at 3 days. (C) Proliferation of different ratios of co-cultured BMSCs and EPCs on SF membranes as detected by CCK-8 assays at 1, 3 and 5 days (n=3).

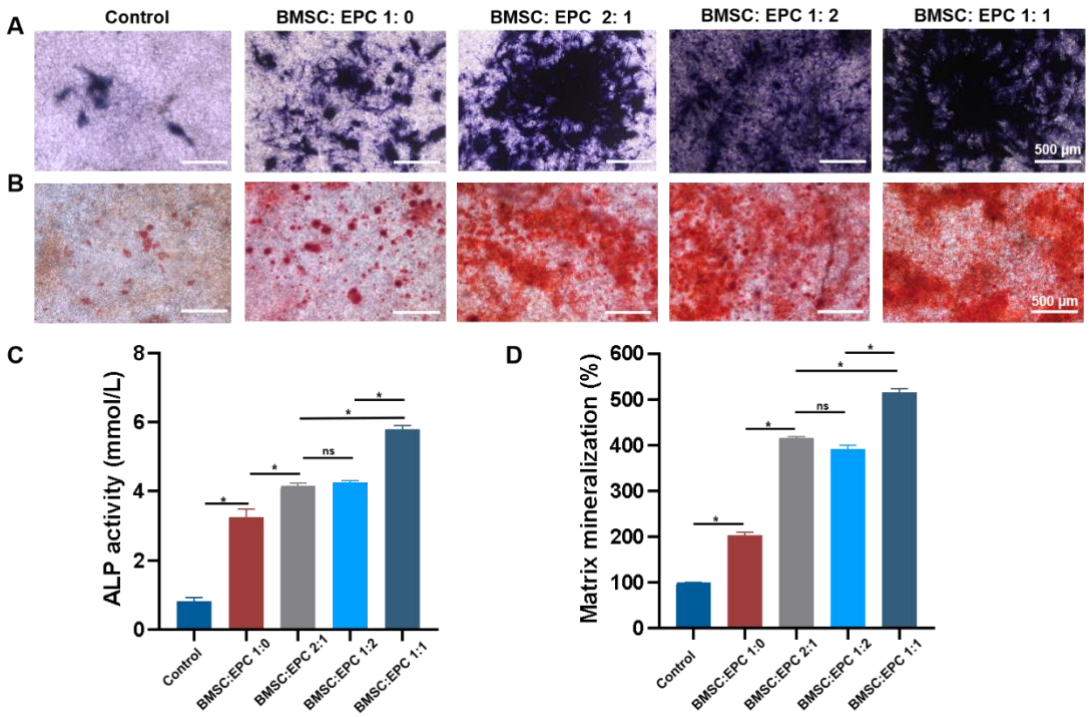

Figure 3. *In vitro* osteogenic differentiation of BMSCs and EPCs co-cultured on electrospun SF membranes. (A) Representative images of ALP staining on day 7. (B) Representative images of AR staining showing calcium deposits on day 14. (C) Quantitative analysis of ALP staining and (D) AR staining. *, $p < 0.05$; ns, no significant difference. n=3.

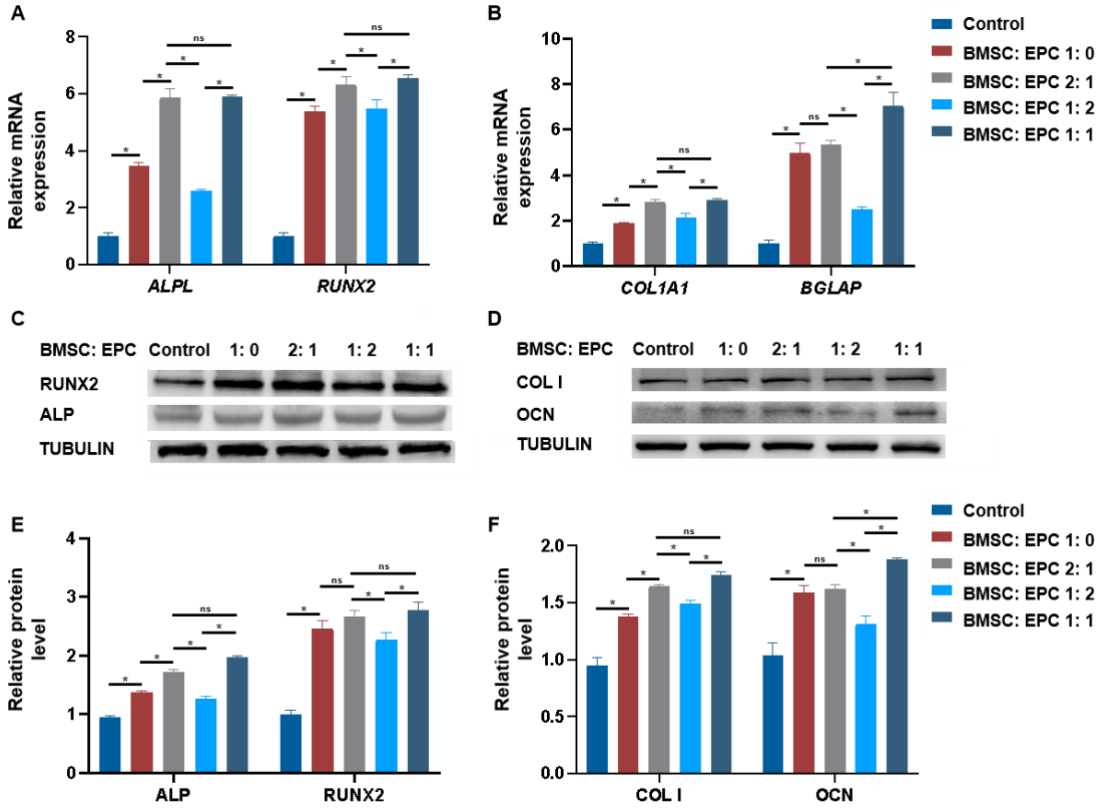

Figure 4. Evaluation of *in vitro* osteogenic differentiation of BMSCs and EPCs co-cultured on electrospun SF membranes. (A) The expression of *ALPL* and *RUNX2* mRNAs on day 7 and (B) *COL1A1* and *BGLAP* mRNAs on day 14, as detected by qRT-PCR. (C) Representative Western blot images showing the abundance of ALP and RUNX2 proteins on day 7 and (D) COL I and OCN proteins on day 14. (E, F) The quantitative analysis of Western blot images in panels C and D. *, $p < 0.05$; ns, no significant difference. n=4.

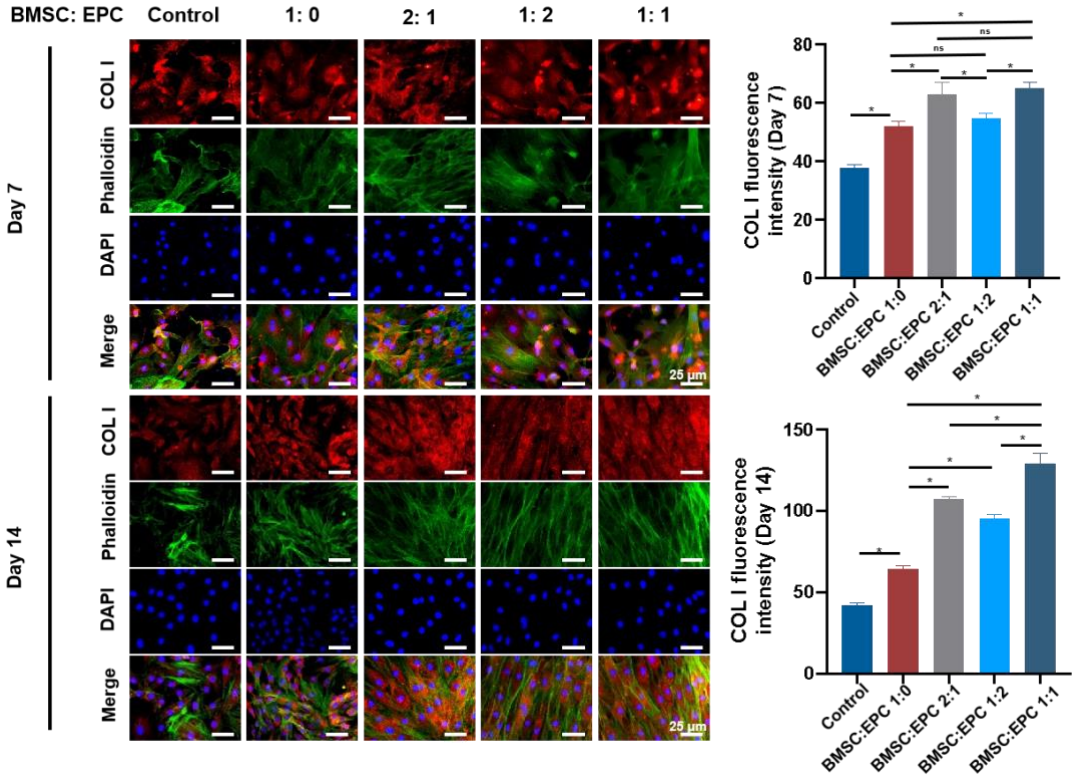

807

808 **Figure 5.** Immunofluorescence images of COL I staining of BMSCs and EPCs co-

809 cultured on electrospun SF membranes. Staining was carried out on day 7 and day 14 of

810 after seeding cells. *, $p < 0.05$; ns, no significant difference. n=3.

811

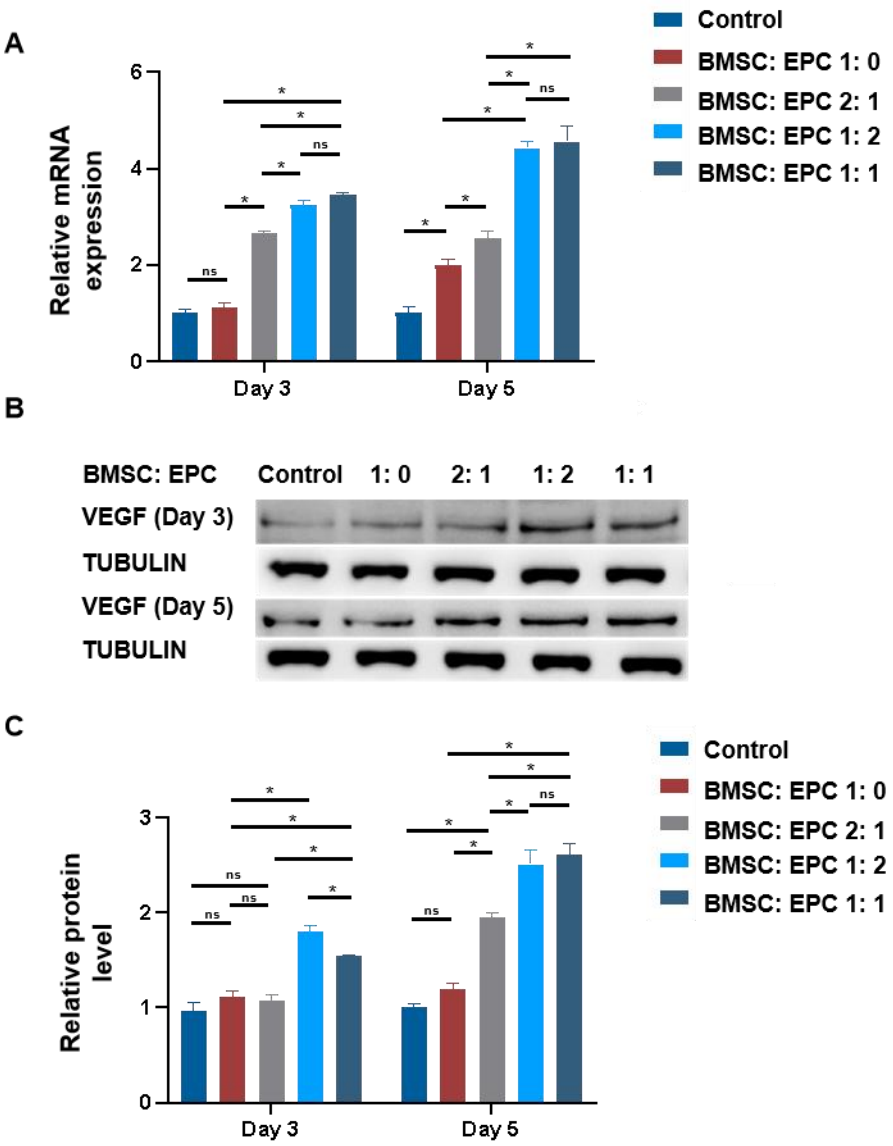

Figure 6. Evaluation of the angiogenesis ability of BMSCs and EPCs co-cultured on electrospun SF membranes. (A) The expression of *VEGF* mRNA was measured on day 3 and 5. (B) Protein expression of VEGF on day 3 and 5 detected by Western blot. (C) Quantitative image analysis of VEGF Western blot. *, $p < 0.05$; ns, no significant difference. n=4.

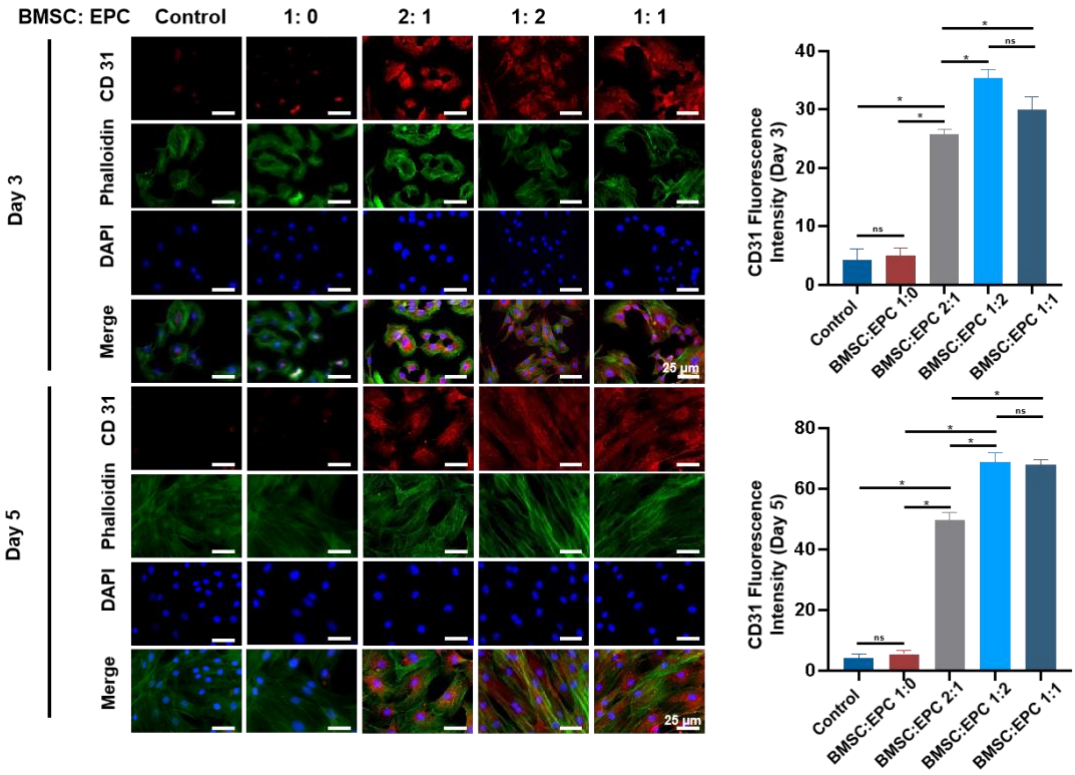

Figure 7. Immunofluorescence images of CD31 staining of BMSCs and EPCs co-cultured on electrospun SF membranes. Staining was carried out on day 3 and 5 after seeding cells. *, $p < 0.05$; ns, no significant difference. n=3.

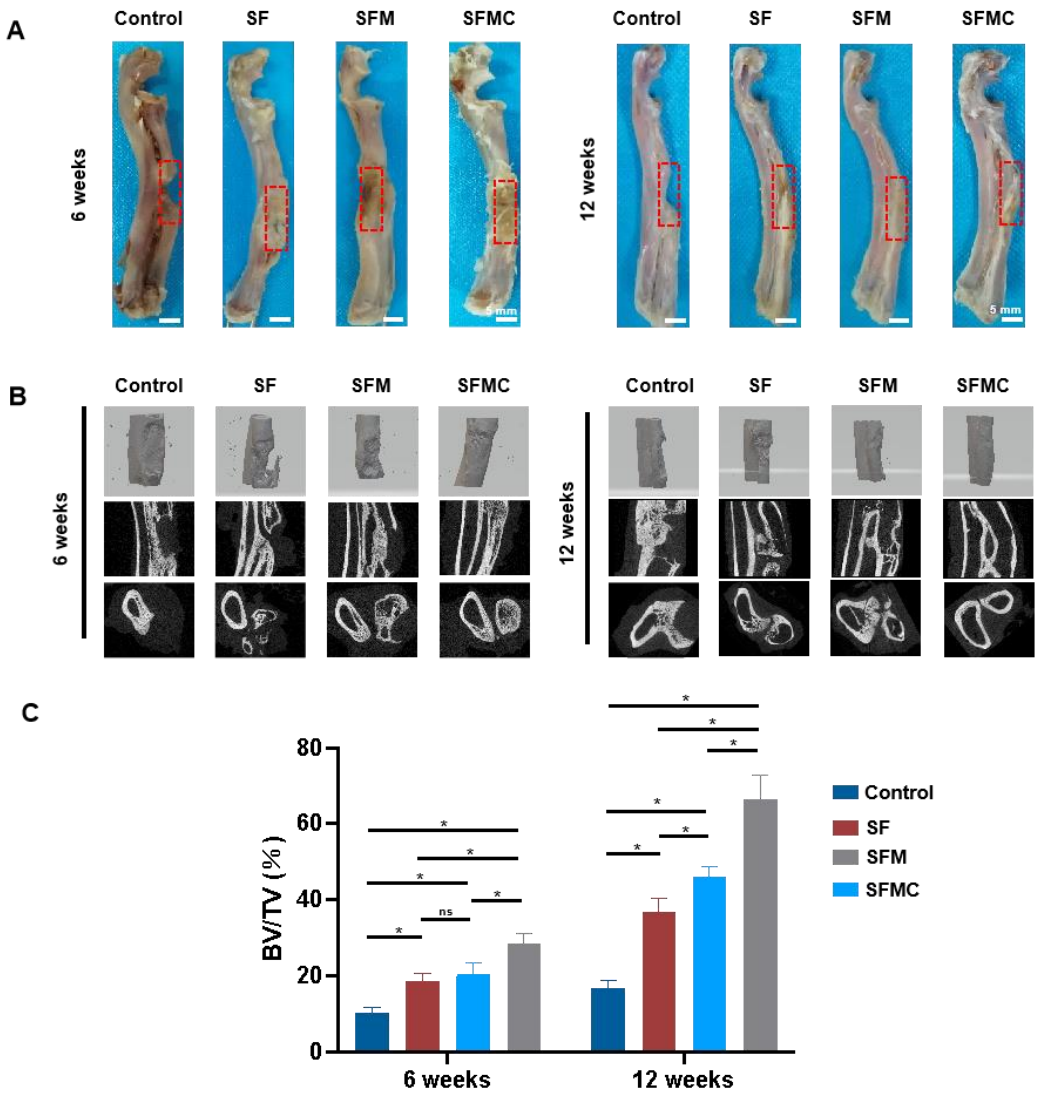

Figure 8. *In vivo* bone repair. (A) Gross visual appearance of bone defects at 6 and 12 weeks after surgery. Red boxes mark the area of initial bone defects. (B) Representative micro-CT 3D images (top row), longitudinal images (middle row) and cross-sectional images (bottom row) of the radius of control, SF, SFM, and SFMC groups at 6 and 12 weeks. (C) BV/TV values in the different groups at 6 and 12 weeks. *, $p < 0.05$; ns, no significant difference. n=3.

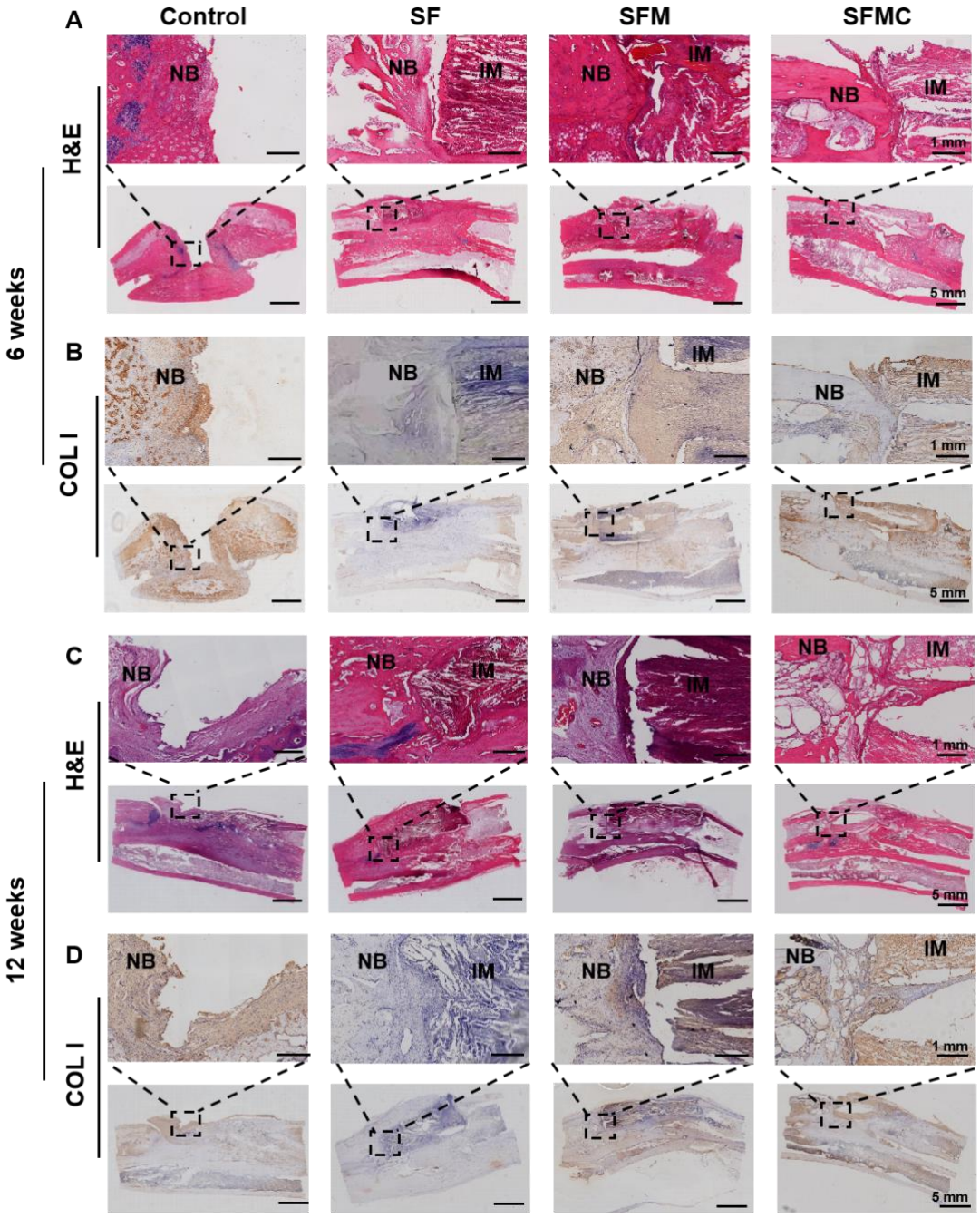

Figure 9. Microscopic features of new bone structures. Representative images of H&E staining of regenerative bone from different groups at 6 weeks (A) and 12 weeks (C) after implantation. Immunohistochemistry staining of COL I at 6 weeks (B) and 12 weeks (D) (n=3). SF indicates the transplantation of SF scaffolds alone. SFM: Scaffolds + cell free

837 electrospun SF membrane. SFMC: Scaffolds + cell contained SF membrane. Control
838 animals received no implants. IM, implanted material; NB, new bone.
839
840

841 Table 1. Primer sequences used for qRT-PCR.

Gene	Forward (5'-3')	Reverse (5'-3')
COL1A1	CAGGCTGGTGTGATGGGATT	CCAAGGTCTCCAGGAACACC
ALPL	TATGTCTGGAACCGCACTGAA	CACTAGCAAGAAGAAGCCTTT
RUNX2	ATCCAGCCACCTTCACTTACA	GGGACCATTGGGAACTGATAG
BGLAP	AACGGTGGTGCCATAGATGC	AGGACCCTCTCTCTGCTCAC
VEGF	CGAGTACATATTCAAGCCTTCC	CTTGCTCTGTCTTTCTTTGGTCC
GAPDH	ATGGTGAAGGTCGGAGTGAA	CCTCGCTCCTGGAAGATGGT

842